Journal of Solid State Chemistry 182 (2009) 2822–2828

Contents lists available at ScienceDirect

Journal of Solid State Chemistry

journal homepage: www.elsevier.com/locate/jssc

Mechanism for the formation of tin oxide nanoparticles and nanowires inside the mesopores of SBA-15

G. Satishkumar, L. Titelman, M.V. Landau *

Blechner Center for Industrial Catalysis and Process Development, Department of Chemical Engineering, Ben-Gurion University of the Negev, Beer-Sheva 84105, Israel

ARTICLE INFO

Article history:
Received 29 April 2009
Received in revised form
18 July 2009
Accepted 22 July 2009
Available online 30 July 2009

Keywords:
Tin oxide
Nanowires
Nanoparticles
SBA-15
Silanols
Nanocasting

ABSTRACT

The formation of polycrystalline tin oxide nanoparticles (NP) and nanowires was investigated using nanocasting approach included solid–liquid strategy for insertion of $SnCl_2$ precursor and SBA-15 silica as a hard template. HR-TEM and XRD revealed that during the thermal treatment in air 5 nm tin oxide NP with well defined Cassiterite structure were formed inside the SBA-15 matrix mesopores at 250 °C. After air calcination at 700 °C the NP assembled inside the SBA-15 mesopores as polycrystalline nanorods with different orientation of atomic layers in jointed nanocrystals. It was found that the structure silanols of silica matrix play a vital role in creating the tin oxide NP at low temperature. The pure tin chloride heated in air at 250 °C did not react with oxygen to yield tin oxide. Tin oxide NP were also formed during the thermal treatment of the tin chloride loaded SBA-15 in helium atmosphere at 250 °C. Hence, it is well evident that silanols present in the silica matrix not only increase the wetting of tin chloride over the surface of SBA-15 favoring its penetration to the matrix pores, but also react with hydrated tin chloride according to the proposed scheme to give tin oxide inside the mesopores. It was confirmed by XRD, N_2-adsorption, TGA-DSC and FTIR spectra. This phenomenon was further corroborated by detecting the inhibition of SnO_2 NP formation at 250 °C after inserting the tin precursor to SBA-15 with reduced silanols concentration partially grafted with tin chloride.

1. Introduction

A series of mesoporous metal oxides have been successfully synthesized through nanocasting strategy, after Ryoo's group reported the synthesis of ordered mesoporous carbon using mesostructured silica as hard template [1]. Zhao et al. [2], first reported the synthesis of ordered mesoporous metal oxides including In_2O_3, Co_3O_4, Cr_2O_3, Fe_2O_3 by utilization of various mesoporous silica with cubic (*Ia*3*d*, *Im*3*m*) or 2-dimensional hexagonal (SBA-15, *p*6*mm*) phases as structure matrices. Usually, in nanocasting strategy the metal nitrates precursors are inserted into the mesopores of silica in dissolved state (e.g. in ethanol) followed by evaporation of solvent [3,4]. The [metal oxide–mesostructured matrix] composite can be prepared also by simple physical mixing of the precursor with mesoporous silica (solid–liquid route) [5–8]. During the heating of the precursor to its melting temperature it penetrates into the mesopores of silica through capillary action followed by decomposition at high temperature to form the metal oxide. Yue and Zhou [8] clearly demonstrated that in order to synthesize mesoporous metal oxide through solid–liquid method the metal nitrate precursor must have a melting point lower than its decomposition temperature. The solid–liquid method is preferable yielding higher integrity of target oxide nanocasts since it excludes the filling of pores with the solvent and does not require multiple impregnations to reach critical metal loading necessary for integrity of nanocasts. Unlike impregnation, solid–liquid method yields monocrystalline metal oxide nanowires with good integrity due to the dense packing of the melted precursor inside the mesopores before it decomposes [9]. In the synthesis of mesoporous metal oxide by hard template technique a shift in the oxide formation towards the lower temperature was observed [3,4]. It was explained as a result of high dispersion of metal precursor over the silica scaffold which accelerates the kinetics of the decomposition of smaller crystals inside the matrix compared with the bulk precursor.

Due to the fact that tin oxide is an n-type semiconductor with wide band gap ($E_g = 3.6$ eV) it has been widely investigated in the areas of gas sensors, solar cells, and catalysts [10–13]. Few literatures are available for the synthesis of mesoporous tin oxide by nanocasting technique using mesoporous silica as hard template. Smatt et al. [14,15] recently synthesized tin oxide monoliths and spheres with hierarchical pore structure using hierarchically porous silica monoliths and spheres as hard templates. Synthesis of mesostructured tin oxide by nanocasting pathway using SBA-15, KIT-6, SBA-16 and spherical mesoporous silica as hard templates was also reported [16,17]. In the synthesis

* Corresponding author.
E-mail address: mlandau@bgu.ac.il (M.V. Landau).

0022-4596/$ - see front matter © 2009 Elsevier Inc. All rights reserved.
doi:10.1016/j.jssc.2009.07.039

of mesostructured tin oxide by nanocasting pathway the common precursors are tin chlorides since tin nitrate is not available. In contrast to the other mesoporous metal oxides prepared using nitrate precursors, only polycrystalline tin oxide nanowires were obtained at high temperature [14,16,17]. Furthermore, in the case of metal nitrates the oxygen for the metal oxide formation is available from the precursor itself. For metal chloride precursors it is unclear whether silanols, reaction medium or coordinated water molecules act as an oxygen source. Understanding of SnO_2 formation mechanism is important for selecting the right strategy controlling its assembling mode and integrity of oxide assembles in corresponding nanocasts.

In the present work, polycrystalline tin oxide NP and nanowires were synthesized using SBA-15 as a hard template through solid–liquid method by nanocasting pathway. The experiments were carried out in air and inert atmosphere at 250–700 °C for tin chloride deposited over pure SBA-15 and Sn-grafted SBA-15 in order to understand the solid state reactions occurred between the hydrated tin chloride and silica scaffold. The materials obtained were characterized by XRD, HR-TEM, N_2-adsorption, TGA-DSC and FT-IR techniques. The experimental results revealed that interaction of tin chloride with the SBA-15 matrix is not the same as with metal nitrates, and the mesoporous oxide formation follows different mechanism. Based on the collected data a reaction scheme was proposed for the creation of nanocrystalline tin oxide at different assembling modes inside the mesopores of SBA-15 by solid–liquid route.

2. Experimental

2.1. Synthesis of tin oxide loaded SBA-15 and nanocast

All chemicals purchased from Aldrich were analytically pure. The SBA-15 was prepared according to the method described in literature [18]. To obtain a tin oxide-SBA-15 composite (Sn–SBA), first 0.5 g of SBA-15 was dispersed in hexane and the solution is stirred at 50 °C. Tin chloride corresponding to 65 wt% of SnO_2 loading was added slowly to the solution. Stirring continued till all the hexane gets evaporated. Finally the sample was dried in air overnight at 80 °C. Afterwards, the resulting material was heated in a ceramic crucible in muffle furnace at 250 and 700 °C for 4 h at the heating rate of 1 °C min^{-1}. The thermal treatment of SBA-15 loaded with tin chloride was also carried out under helium flow in a tubular furnace at 250 and 700 °C for 4 h. Finally the silica matrix was removed by dissolution in 10% HF overnight at room temperature.

Tin chloride grafted SBA-15 (SBA–SnG) was obtained by following the procedure reported in literature [19]. Briefly, calcined SBA-15 was slurried in absolute ethanol solution containing the excess of anhydrous tin chloride for 1 h at 60 °C. The material was then washed with absolute ethanol and dried in air oven overnight at 80 °C. The so obtained SBA–SnG material was loaded with tin chloride at amount corresponding to 65 wt% of SnO_2 as in the case of as-synthesized SBA-15. This material denoted as Sn–SBA–SnG was heated in helium atmosphere at 250 °C for 4 h.

2.2. Materials characterization

The chemical composition of the materials was measured by energy dispersive X-ray spectroscopy (EDX) analysis with a JEOL JEM 5600 scanning electron microscope. Average of five data points at different locations of the solid was registered.

Wide-angle XRD patterns were obtained with a Philips 1050/70 powder diffractometer fitted with a graphite monochromator; software developed by Crystal Logic was used. Phase identification was performed by using BEDE ZDS computer search match program coupled with ICDD (International Center for Diffraction Data) Powder Diffraction File database (2006). The data were collected in a range of 2θ values from 10° to 80° with a step size of 0.05°. The (110) reflection for SnO_2 ($2\theta = 26.6°$), (002) for $SnCl_2$ ($2\theta = 19.2°$), (100) and (110) for $SnCl_2 \cdot 2H_2O$ ($2\theta = 10.5°$ and 16.1°), (200) for $Sn_4(OH)_6Cl_2$ ($2\theta = 17.4°$), (11.15 and 12.11) for $Sn_{21}Cl_{16}(OH)_{14}O_8$ ($2\theta = 35.4°$) phases were selected to determine their crystalline size. The crystal size was determined by using Scherrer equation $h = K\lambda/[(B^2-\beta^2)^{0.5}\cos(2\theta/2)]$, where $K = 1.000$ is the shape factor, $\lambda = 0.1541$ nm; β is the instrumental broadening; B is the experimental peak broadening corresponding to the selected reflections. Low angle XRD patterns were recorded using (1/12)°-divergence slit and 1/30 mm-receiving slit.

Surface area, pore volume and pore size distribution were obtained from N_2 adsorption–desorption isotherms, by using the conventional BET and BJH methods. The last two characteristics were calculated using desorption branch of the isotherm. The samples were outgassed under vacuum for 2 h at 250 °C. Isotherms were obtained at the temperature of liquid nitrogen with a NOVA-2000 (Quantachrome, Version 7.02) instrument.

The infrared spectra were recorded with a Nicolet Impact 460 FTIR spectrometer, with the use of KBr pellets (0.005 g sample and 0.095 g KBr), with 32 sample scans. The data were treated with OMNIC software. The thermal decomposition of the material was analyzed by thermogravimetric analysis (TGA) and differential scanning calorimetry (DSC) over a temperature range from room temperature to 600 °C with TG-50-Mettler-Toledo and Mettler-Toledo-DSC 823e instruments, respectively. The measurements were carried out in a flow of nitrogen at a heating rate of 5 °C min^{-1}.

HRTEM (high resolution transmission electron microscopy) analysis was conducted on a FasTEM JEOL 2010 microscope operating at 200 kV. The samples for HRTEM were prepared by depositing a drop of ultrasonicated ethanol suspension of solid material on a carbon-coated copper grid.

3. Results and discussion

3.1. Synthesis of tin oxide NP and polycrystalline tin oxide nanowires

The low-angle XRD patterns of as-synthesized SBA-15 silica displayed a high intensity peak (100) with a d-spacing of 10.5 nm and two less intensive reflections with d-values consistent with hexagonal arrangement of the pores (Fig. 1). The as-synthesized SBA-15 silica had total BET surface area 817 $m^2 g^{-1}$, pore volume 1.00 $cm^3 g^{-1}$ and average pore diameter 5.5 nm in agreement with low angle XRD and HRTEM data. The surface area associated with micropores estimated by the t-plot method was 261 $m^2 g^{-1}$.

The Sn/Si = 0.92 and Cl/Sn = 1.94 atomic ratios measured by EDX analysis in the Sn–SBA material dried at 80 °C were consistent with existence of tin in form of $SnCl_2$ which corresponds to 65 wt% SnO_2 in SnO_2/SiO_2 composite after calcination at 700 °C. - Fig. 2 shows the wide angle XRD patterns of different phases in Sn–SBA material formed during the thermal treatment in air. The sample dried at 80 °C was characterized by reflections corresponding to tin chloride of particle size more than 50 nm (ICDD Card no. 72-137), which indicates the presence of tin chloride at the outer surface of SBA-15 micrograins. After heating at 250 °C, the X-ray diffractogram displayed patterns of tin oxide phase (Cassiterite) with 4 nm particle size (ICDD Card no. 5-467).

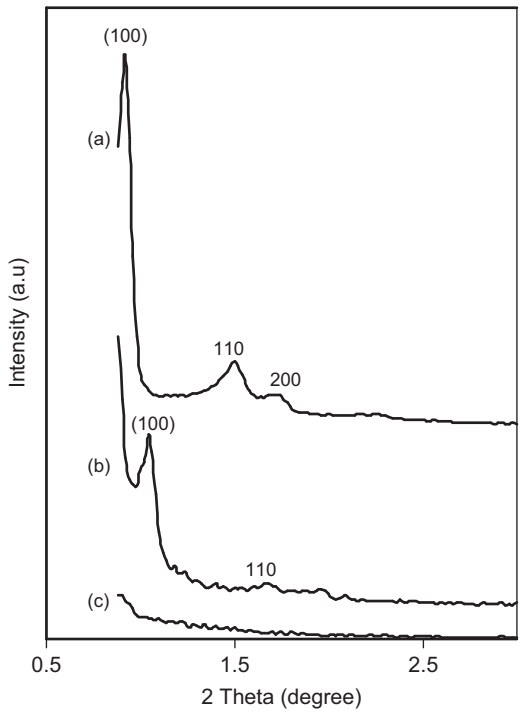

Fig. 1. Low-angle XRD patterns of (a) SBA-15, (b) SnO_2 obtained after removal of silica from composite calcined in air at 700 °C, and (c) SnO_2 obtained after removal of silica from composite calcined in air at 250 °C.

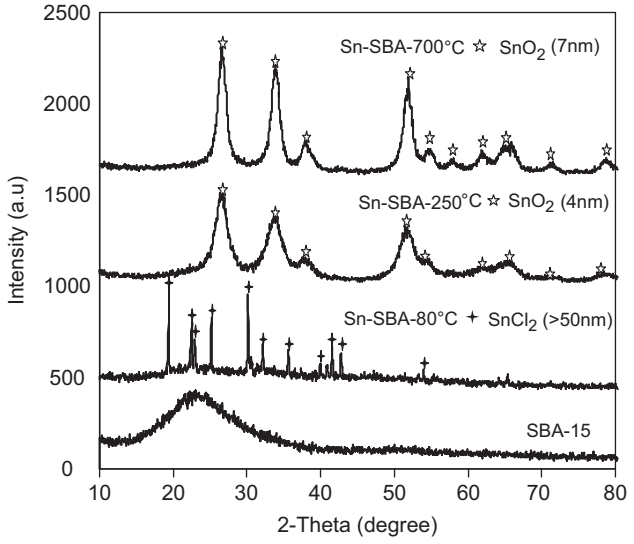

Fig. 2. XRD patterns of SBA-15 and Sn–SBA heated at various temperatures in air.

HR-TEM micrographs of Sn/SBA-15 material obtained at 250 °C in air before and after removal of silica matrix are shown in Fig. 3. They demonstrated formation of small tin oxide NP inside the pores of SBA-15. The HRTEM micrographs revealed that tin oxide appeared in SBA-15 matrix as NP aligned along the nanotubular pores (Fig. 3(A)), and upon removal of silica matrix (Sn/Si = 14.8) did not show any ordering inside their aggregates (Fig. 3(B)). The last conclusion was consistent with the absence of XRD reflections at low angles of $2\theta < 5^\circ$ as shown Fig. 1.

When the Sn–SBA composite was heated at 700 °C in air the shape of XRD patterns corresponding to SnO_2 phase further altered demonstrating peaks narrowing corresponding to the growth of average particle size to 7 nm (Fig. 2d). The tin oxide survived the nanowires shape-ordering and maintained the integrity of Sn/SBA precursor after removal of silica scaffold (Sn/Si = 15.9, Fig. 3(D)). This reflects the formation of grain boundaries between the jointed SnO_2 NP at 700 °C strengthening the nanowires. The low angle XRD patterns of SnO_2 nanocast obtained after calcination of Sn–SBA at 700 °C demonstrated in Fig. 1 consistent with formation of mesostructured tin oxide.

The textural properties of Sn–SBA-15 material heated at different temperatures and atmospheres were listed in Table 1. The surface area and the pore volume of Sn–SBA heated at 250 °C in air decreased considerably compared with the parent SBA-15 that implies the formation of tin oxide NP inside the mesopores of SBA-15 at that temperature. It is further proved from the nitrogen sorption isotherms of the sample which shows a clear shift in the capillary condensation loop towards the low P/P_0 values (Fig. 4(A)). After calcination in air at 700 °C, the sintering and arrangement of SnO_2 NP in nanowires caused an increase in surface area (Table 1). In addition to that, the increase in mesopore and decrease in micropore surface area with rising of calcination temperature (Table 1) implies partial jointing of NP located in parallel nanotubular mesopores of SBA-15 being a reason for integrity of nanowires after matrix removal. This effect was observed in the HRTEM images of SnO_2 replica demonstrating good integrity of nanowires that survived the align after scaffold removal as shown in Fig. 3. SnO_2 replica obtained after the removal of silica shows typical type IV isotherm with hysteresis loops, which indicates the formation of well-defined mesostructure (Fig. 4(A)). Narrow pore size distribution of SnO_2 replica and its relatively high surface area of 75 $m^2 g^{-1}$ further proved the ordered mesostructure of the obtained material (Fig. 4(B)).

If $SnCl_2$ located at the external surface of SBA-15 micrograins would decompose without melting it should yield large nonporous crystals outside the matrix pores. If the precursor melts first and then decomposes after penetration into porous system of the matrix it should give single crystal porous mesostructured metal oxide as demonstrated in [16]. In our case the melting and decomposition of the $SnCl_2$ precursor occurred simultaneously that resulted in polycrystalline porous metal oxide. Based on the observation that tin oxide NP are formed in $SnCl_2$–SBA-15 composite at low temperature of 250 °C whereas the bulk tin chloride is stable in air at 250 °C, it can be assumed that some specific chemical transformations of $SnCl_2$ occur after its contacting with the silica matrix at this temperature. These transformations can involve oxygen from ambient air, silanols or crystallization water molecules by heating in inert atmosphere. The identification of the oxygen source for formation of tin oxide from its chloride precursor was investigated in additional experiments.

3.2. Effect of silanols

It was decided to compare the state of tin in Sn–SBA composite after heating it to 250–700 °C in air and inert atmosphere (He). In inert atmosphere the tin chloride resided over the external surface of SBA-15 micrograins should melt at 250 °C and penetrate to the matrix pores through capillary action without decomposition. Surprisingly, the reflections characteristic for tin oxide (ICDD Card no. 5-467) appear together with reflections of other intermediate phases when the sample was heated at 250 °C for 1 h (Fig. 5b) and only tin oxide peaks of 4 nm particle size were observed when it was kept at the same temperature for 4 h in Helium atmosphere (Fig. 5c). Heating to 700 °C in helium atmosphere did not change

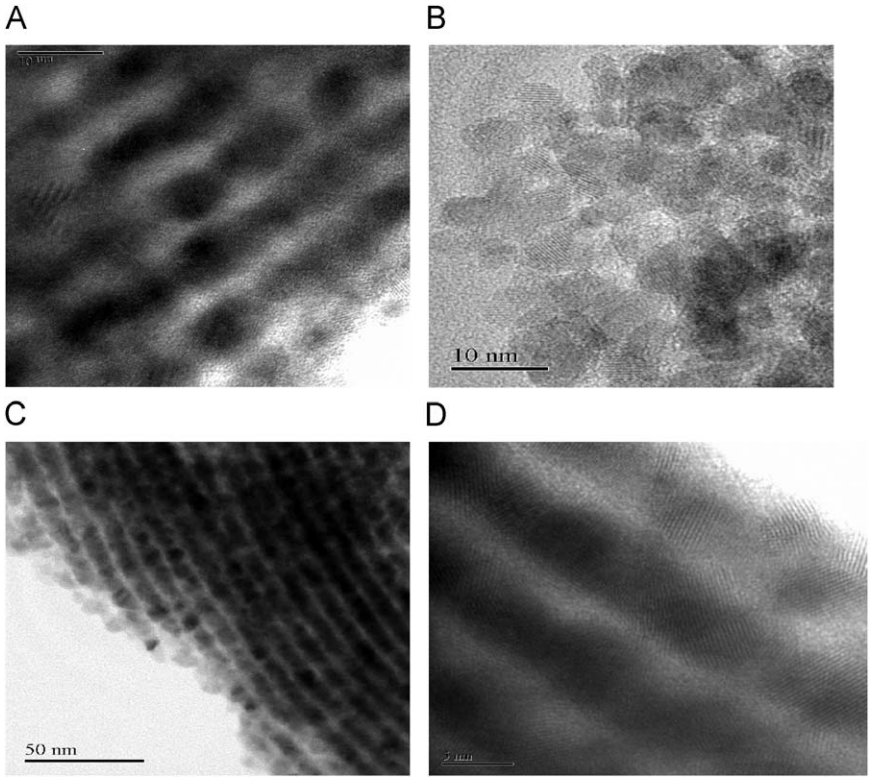

Fig. 3. HRTEM micrographs of SnO_2 NP obtained at 250 °C (A) before and (B) after silica removal and SnO_2 nanowires obtained at 700 °C (C) before and (D) after silica removal.

Table 1
Textural properties of SBA-15, Sn–SBA and SnO_2 replica.

Material	Total surface area($m^2 g^{-1}$)	Mesopore surf. area ($m^2 g^{-1}$)	Micropore surf. area ($m^2 g^{-1}$)	Total pore volume ($cc g^{-1}$)	Micropore volume ($cc g^{-1}$)
SBA-15	817	556	261	1.000	0.121
Sn–SBA-250 °C-4 h-air	204	120	84	0.312	0.042
Sn–SBA-700 °C-6 h-air	250	207	43	0.323	0.019
SnO_2-replica	75	75	–	0.080	–
Sn–SBA-250 °C-1 h-He	102	102	–	0.230	–
Sn–SBA-250 °C-4 h-He	130	130	–	0.261	–

the XRD patterns of tin oxide phase except slight increase in intensity (not shown). In contrast to the tin chloride loaded SBA-15, the pure tin chloride heated in air at 250 °C did not react with oxygen, which resulted in appearance of tin chloride (ICDD Card no. 72-137), hydrated tin chloride (ICDD Card no. 20-1292) and $Sn_4(OH)_6Cl_2$ (ICDD Card no. 15-676) reflections in XRD patterns of the material (Fig. 5a). The above observations clearly indicate that pure tin chloride and tin chloride loaded over SBA-15 are converted according to different mechanisms during the thermal treatment. The transformation of $SnCl_2$–SnO_2 in $SnCl_2$–SBA-15 composite in He excludes participation of air. Direct reaction of $SnCl_2$ with crystallization water molecules to form SnO_2 also should be excluded since it does not proceed even during heating the bulk tin chloride in air. It was assumed that the reason for observed effect is the participation of matrix silanols in the reaction to yield tin oxide. As a result, melting and decomposition of tin chloride occur together and thus led to the formation of polycrystalline nanowires at high temperature.

The density of Si–OH groups on the mesoporous silica has been estimated as 4.0 Si–OH/nm^2 [20]. The assumption of two Si–OH groups in SBA-15 reacting with each $SnCl_2$ unit should give ~28 wt% of tin oxide in the material. The amount of silanols available in the SBA-15 matrix is not enough to oxidize the existing amount of tin corresponding to 65 wt% SnO_2 in the composite. To find the oxygen source for the formation of tin oxide with lack of silanols and in inert atmosphere, we carried out TGA and DSC studies of pure tin chloride and Sn/SBA-15 in inert atmosphere and the results are shown in Fig. 6(A) and 6(B), respectively. TGA plot of pure tin chloride shows only one huge weight loss about 80% from the temperature 300 to 550 °C and a strong exothermic peak was observed at around 240 °C in DSC. This exothermic peak can be attributed to the formation of $Sn_4(OH)_6Cl_2$ phase due to the reaction of tin chloride with water molecules at the melting temperature of tin chloride. XRD results of pure tin chloride heated at 250 °C in air confirmed the presence of $Sn_4(OH)_6Cl_2$ (Fig. 5a) phase supporting the DSC results. The weight loss occurred from 300 to 550 °C was due to the volatilization of some tin (II) chloride at 300 °C and formation of tin (II) oxide from $Sn_4(OH)_6Cl_2$. On further heating the tin (II) oxide formed disproportionate to tin (IV) oxide and β-tin as demonstrated in [21].

Three stages of weight loss were observed for Sn–SBA material in TGA and an exothermic peak was observed in DSC spectra around 370 °C as observed in the literature [7]. The first two stages

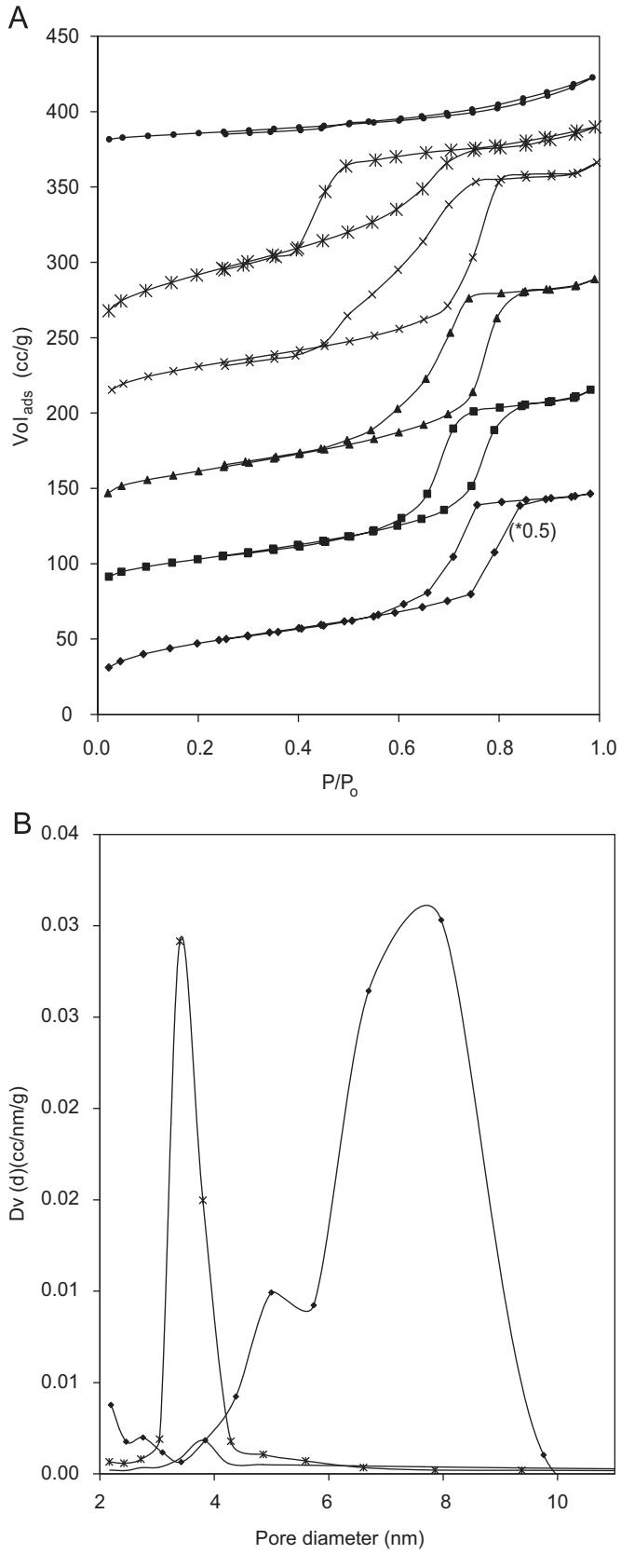

Fig. 4. (A) Nitrogen adsorption isotherm of (♦) SBA-15, (■) Sn–SBA-250 °C-1 h-He, (▲) Sn–SBA-250 °C-4 h-He, (×) Sn–SBA-250 °C-4 h-air, (∗) Sn–SBA-700 °C-4 h-air and (●) SnO_2-replica; (B) pore size distribution of (♦) SBA-15, (∗) Sn–SBA-700 °C-4 h-air and (●) SnO_2-replica.

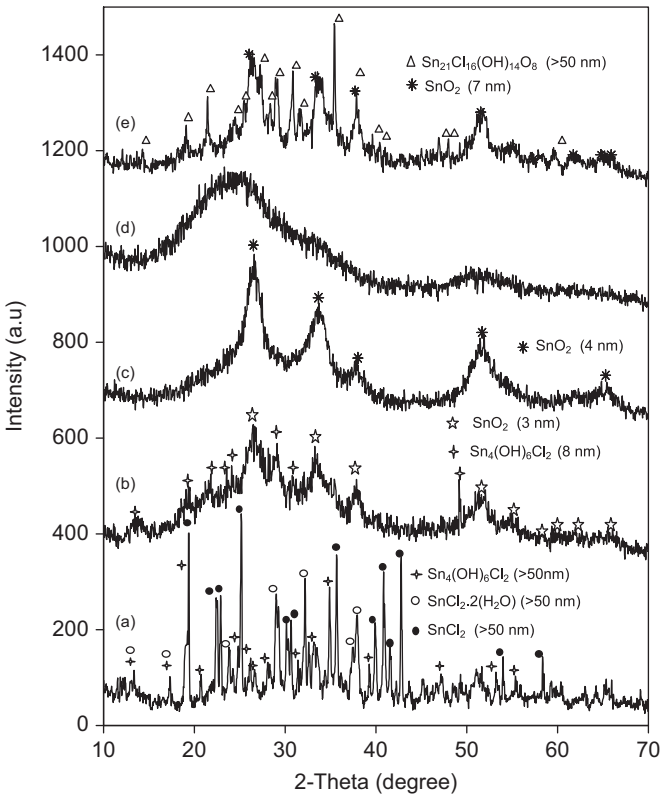

Fig. 5. XRD patterns of (a) $SnCl_2$-250 °C-4 h-air, (b) Sn–SBA-250 °C-1 h-He, (c) Sn–SBA-250 °C-4 h-He, (d) SBA-SnG and (e) Sn–SBA-SnG-250 °C-4 h-He.

up to 15% weight loss up to 180 °C are attributed to the removal of physically adsorbed water molecules, and their corresponding wide endothermic peak was observed in DSC. The third weight loss of about 25% was occurred from 250 to 380 °C. The different patterns of thermograms recorded with bulk $SnCl_2$ and Sn–SBA materials are evident that they follow different transformation routes to yield tin oxide. The observed transformations were explained by the reaction pathway shown in Scheme 1. Tin chloride reacts with surface Si–OH groups of SBA-15 to form grafted SiO–Sn–Cl. The nucleophilic attack of water molecules existed in starting crystallohydrate $SnCl_2 \cdot 2H_2O$ on framework silicon forms HO–Sn–Cl moieties. Coordination of another water molecule with the vacant *p* orbital of tin formed in Sn(2+)-hydroxychloride (HO–Sn–Cl) yields SnO_2, H_2 and HCl by redox transformation as shown in the Scheme 1. The last possibility of SnO_2 formation by exothermic solid–gas redox hydrolysis of Sn(2+)-oxide with the release of hydrogen was recently demonstrated in [22]. Analogously the Sn(2+)-hydroxychloride produced at the first hydrolysis step of grafted tin chloride can undergo the redox hydrolysis at the second step yielding SnO_2NP. The broad exothermic peak observed in DSC spectra of Sn–SBA material at 250–370 °C can be attributed to this reaction. Though the Sn–SBA material heated to 250 °C in He for 1 h contains some $Sn_4(OH)_6Cl_2$ phase along with the tin oxide phase (Fig. 5b), the absence of exothermic peak at 250 °C in DSC spectra of the same sample indicates that the formation of $Sn_4(OH)_6Cl_2$ over SBA-15 is not significant. The FT-IR spectra of SBA-15 and Sn–SBA materials heated in He at 250 °C for 1 h are shown in Fig. 7a and c, respectively. The disappearance of peak at 963 cm^{-1} which is assigned to the presence of defective Si–OH group, after insertion of $SnCl_2$ and heating further prove the participation of silanols in the reaction. The presence of peak at 630 cm^{-1} due to the Sn–O stretching in the spectra of Sn–SBA material confirms the tin oxide formation [23]. The comparison of surface areas of Sn–SBA heated

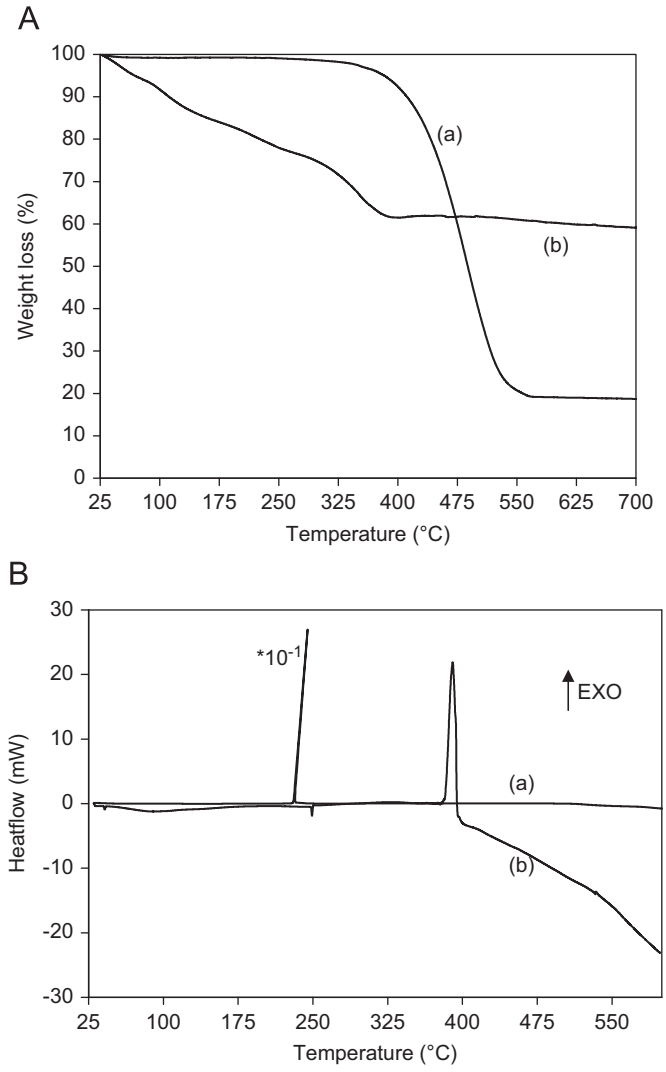

Fig. 6. (A) TGA and (B) DSC curves of (a) $SnCl_2$ and (b) Sn/SBA-15.

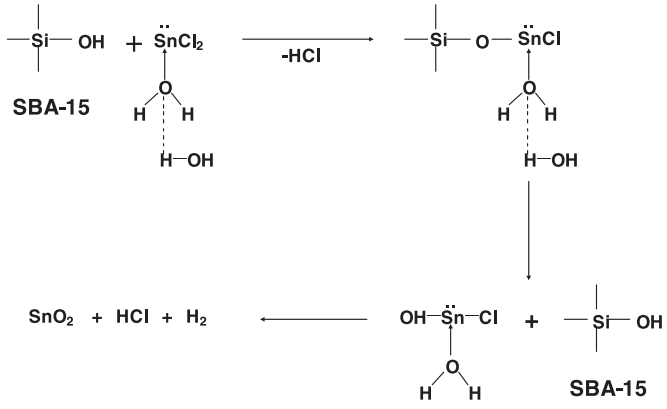

Scheme 1. Reaction scheme for the formation of tin oxide over SBA-15 in inert atmosphere.

at 250 °C in air and He atmospheres (Table 1) showed that both samples differ only in their microporous surface area. In air atmosphere both water molecules and air can act as a source of oxygen which accelerates the kinetics of tin(4+)-oxide formation

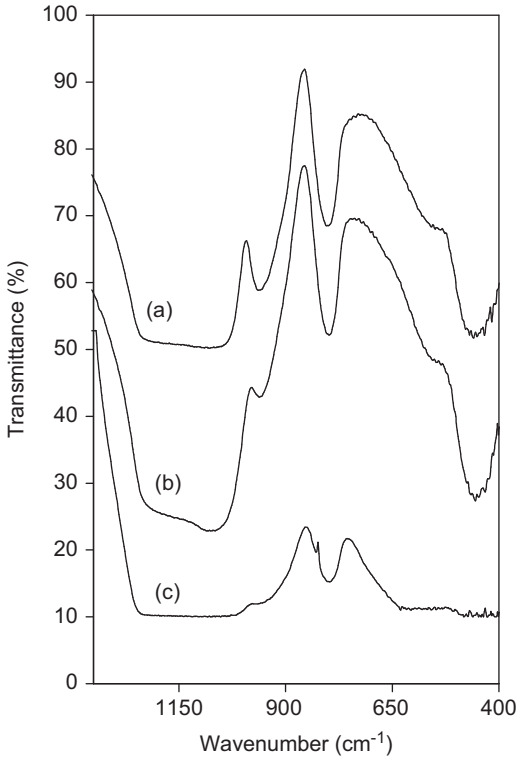

Fig. 7. FT-IR spectra of (a) SBA-15, (b) SBA–SnG and (c) Sn–SBA-250 °C-1 h-He.

that penetrates quickly in to the mesopores through micropores. Whereas, in inert atmosphere the reaction between $SnCl_2$ and water takes place slowly this reduces the penetration rate of tin oxide. Therefore the formed SnO_2 is partially remained in the micropores of SBA-15 matrix. This blocks the micropores reducing the surface area of the material as follows from Table 1.

The above experimental results evidence the vital role of structure silanols in creating the tin(4+)-oxide NP. To confirm the reaction of silanols with tin chloride the same experiment was repeated with the tin chloride grafted Sn–SBA–SnG composite where the silanols were capped by tin chloride. As mentioned earlier in the discussion, we assumed that two Si–OH groups in SBA-15 react with each $SnCl_2$, which correspond to a full monolayer at ~28 wt% Sn. However, after repeating the grafting procedure three times it was confirmed by EDX results that 16 wt% of tin was grafted. The amorphous XRD pattern of grafted SBA-15 sample (Fig. 5d) and the reduction in the peak intensity of 963 cm^{-1} in FT-IR (Fig. 7b) confirmed the grafting of tin chloride over the walls of SBA-15 pores. The wide angle XRD spectrum of Sn–SBA–SnG heated at 250 °C in He for 4 h showed peaks of $Sn_{21}Cl_{16}(OH)_{14}O_6$ (ICDD Card no. 35-907) phase with particle size of 50 nm (Fig. 4e). The existence of big crystals of $Sn_{21}Cl_{16}(OH)_{14}O_6$ phase at the external surface of SBA-15 micrograins implies that the decreasing of silanols concentration strongly reduced the wetting of SBA-15 with tin chloride needed for efficient penetration of $SnCl_2$ inside the pores. It is also evident that the silanols recovery at the first hydrolysis step (Scheme 1) is a slower process than formation of $Sn_{21}Cl_{16}(OH)_{14}O_6$ phase. The existence of small 7 nm NP of tin oxide phase indicates that part of silanols remained in the SBA-15 matrix. The silanols present in the silica matrix not only increase the wetting of tin chloride over the surface of SBA-15 favoring its penetration to the matrix pores, but also react with tin(2+)-chloride to yield an intermediate for the formation of tin(4+)-oxide NP.

4. Conclusions

Polycrystalline tin oxide NP and nanowires were successfully synthesized using SBA-15 as a hard template. From the above study it was confirmed that mechanism of formation of metal oxide by nanocasting method depends upon the nature of the precursor. The yield of polycrystalline tin oxide nanowires is due to the simultaneous melting and decomposition of tin chloride precursor during the thermal treatment. The formation of tin oxide particles in inert atmosphere confirms the reaction of tin chloride with silanols of silica matrix forming an intermediate that yields tin oxide by further reaction with water. This facilitates the tin chloride to decompose as soon as it melts. Based on the collected data a reaction scheme was proposed in which the water molecules coordinated with tin chloride participate in the reactions to yield tin(4+)-oxide nanoparticles in inert atmosphere.

Acknowledgments

This study was supported by Israeli Science Foundation, Grant 739/06. The authors gratefully acknowledge Dr. E. Erenburg for conducting the XRD characterizations and Dr. V. Ezersky for TEM characterization of investigated materials.

References

[1] R. Ryoo, S.H. Joo, S. Jun, J. Phys. Chem. B 103 (1999) 7743–7746.
[2] B. Tian, X. Liu, H. Yang, S. Xie, C. Yu, B. Tu, D. Zhao, Adv. Mater. 15 (2003) 1370–1374.
[3] A. Rumplecker, F. Kleitz, E.L. Salabas, F. Schuth, Chem. Mater. 19 (2007) 485–496.
[4] C. Dickinson, W. Zhou, R.P. Hodgkins, Y. Shi, D. Zhao, H. He, Chem. Mater. 18 (2006) 3088–3095.
[5] Y.M. Wang, Z.Y. Wu, L.Y. Shi, J.H. Zhu, Adv. Mater. 17 (2005) 323–327.
[6] Y.M. Wang, Z.Y. Wu, J.H. Zhu, J. Solid State Chem. 177 (2004) 3815–3823.
[7] Q. Jiang, Z.Y. Wu, Y.M. Wang, Y. Cao, C.F. Zhou, J.H. Zhu, J. Mater. Chem. 16 (2006) 1536–1542.
[8] W. Yue, W. Zhou, Chem. Mater. 19 (2007) 2359–2363.
[9] M.V. Landau, L. Vradman, in: V. Valtchev, S. Mintova, M. Tsapatis (Eds.), Ordered Porous Solids, Elsevier, Amsterdam, 2009, p. 680.
[10] Z. Liu, D. Zhang, S. Han, C. Li, T. Tang, W. Jin, X. Liu, B. Lei, C. Zhou, Adv. Mater. 15 (2003) 1754–1757.
[11] Y. Liu, J. Dong, M. Liu, Adv. Mater. 16 (2004) 353–356.
[12] Z.R. Dai, Z.W. Pan, Z.L. Wang, J. Am. Chem. Soc. 124 (2002) 8673–8680.
[13] J.Q. Hu, X.L. Ma, N.G. Shang, Z.Y. Xie, N.B. Wong, C.S. Lee, S.T. Lee, J. Phys. Chem. B 106 (2002) 3823–3826.
[14] J.H. Smatt, C. Weidenthaler, J.B. Rosenholm, M. Linden, Chem. Mater. 18 (2006) 1443–1450.
[15] J.H. Smatt, N. Schuwer, M. Jarn, W. Lindner, M. Linden, Micro. Meso. Mater. 112 (2008) 308–318.
[16] H. Kim, J. Cho, J. Mater. Chem. 18 (2008) 771–775.
[17] J.K. Shon, S.S. Kong, Y.S. Kim, J.H. Lee, W.K. Park, S.C. Park, J.M. Kim, Micro. Meso. Mater. 120 (2009) 441–446.
[18] D. Zhao, J. Feng, Q. Huo, N. Melosh, G.H. Fredrickson, B.F. Chmelka, G.D. Stucky, Science 279 (1998) 548–552.
[19] R. Ryoo, S. Jun, J.M. Kim, M.J. Kim, Chem. Commun. (1997) 2225–2226.
[20] I.G. Shenderovich, G. Buntkowsky, A. Schreiber, E. Gedat, S. Sharif, J. Albrech, N.S. Golobev, G.H. Findenegg, H. Limbach, J. Phys. Chem. B 107 (2003) 11924–11939.
[21] J.D. Donaldson, W. Moser, W.B. Simpson, J. Chem. Soc. (1963) 1727–1731.
[22] S. Abanades, P. Charvin, F. Lemont, G. Flamant, Int. J. Hydrogen Energy 33 (2008) 6021–6030.
[23] S. Jouen, B. Lefez, M.T. Sougrati, B. Hannoyer, Mater. Chem. Phys. 105 (2007) 189–193.